Reinforced high-strength concrete square columns confined by aramid FRP jackets. part II: modeling

Han-liang Wu[1,2], Yuan-feng Wang[1]*, and Yi-shuo Ma[1]

[1]School of Civil Engineering, Beijing Jiaotong University, Beijing, 100044, PR China.
[2]Bridge Technology Research Center, Research Institute Center of Highway,
Ministry of Transportation, Beijing, 100088, PR China.

Abstract.   Based on the experimental data presented in part I of these companion papers, a semi-empirical model is proposed for axial stress-strain curves of reinforced high-strength concrete square columns confined by aramid fiber reinforced polymer (FRP) jackets. Additionally, a three-dimensional finite element model is developed to simulate the mechanical behaviors of the columns. In the finite element model, both material nonlinear and contact nonlinear are taken into account. Moreover, the influence of contact nonlinear (i.e., the end friction on the contact surface between test machines and specimens) is investigated deeply. Predictions from both the semi-empirical model and the finite element model agree with the experimental results, and it is also demonstrated that the friction coefficient of end friction notably affect the properties of columns when it ranges from 0.00 to 0.25.

Keywords: reinforcement; high-strength concrete (HSC); confined columns; fiber reinforced polymers (FRP); finite element analysis; end friction.

1. Introduction

Accompanied with wide applications of fiber reinforced polymer (FRP) composites in civil engineering, the need of further understanding on properties of FRP-retrofitted structures is becoming more and more exigent for the aim of ensuring the safety of the structures. Since it is difficult to make certain the mutual effects among concrete cores, internal steel reinforcements, and external FRP jackets, the mechanical behaviors of FRP-confined reinforced concrete (RC) columns are hard to be predicted. As important as experimental investigations which are valuable in studying the properties of FRP-confined RC columns, modeling is also indispensable for deeply understand their mechanical properties.

In recent years, researchers have proposed some empirical or semi-empirical models (Samaan *et al.* 1998, Xiao and Wu 2000, Mukherjee *et al.* 2004, Youssef *et al.* 2007, Wu and Wang 2010) and analytical models for FRP-confined plain concrete columns [including elastic models (Braga *et al.* 2006 Campione 2008), nonlinear elastic models (Fujikake *et al.* 2004, Montoya *et al.* 2004), elastic-plastic models (Deniaud and Neale 2006), and plastic models (Karabinis and Rousakis 2002)]. Although the analytical models provide stronger theoretical bases, the empirical or semi-empirical models are more convenient for use. However, for FRP-confined RC columns, it is a problem to make certain the attributions of internal

steel stirrups and external FRP jackets. Some researchers resolved this problem by means of superimpose the confining stresses attributed to internal steel stirrups and external FRP jackets (Harajli 2006, Debaiky *et al.* 2007), or accumulating the contributions of internal steel stirrups and external FRP jackets to load capacity of the columns (Li *et al.* 2003, Lin and Liao 2004, Maalej *et al.* 2003, Wang and Hsu 2008).

As a widely used numerical method, finite element analysis (FEA) can consider material, geometric, and contact nonlinearities. In the past decade, by using FEA software, many researchers have successfully modeled FRP-confined plain or RC columns under monotonic axial loading (Mirmiran *et al.* 2000, Grassl 2004, Malvar *et al.* 2004, Montoya *et al.* 2004, Parvin and Wang 2001, Mosalam *et al.* 2007, Eid and Paultre 2007), or cyclic axial compressive loading (Mirmiran *et al.* 2000), or cyclic lateral loading (Parvin and Jamwal 2006, Rougier and Luccioni 2007). However, it should be pointed out that the friction on contact surfaces between load platens (two steel plates) of testing machine and compressed specimens, which is named as the end friction, was not considered in previous studies. In practice, the end friction is unavoidable in conventional experiment. For concrete columns under axial compressive loading, the end friction provokes an additional lateral confinement in top and bottom regions of columns. The additional lateral confinement results that the concrete in the top and bottom regions has higher compressive strength and smaller lateral dilation than those in the mid-height regions of columns, which is a main reason why the failure of columns always appear firstly in the mid-height regions. Further more, the end friction has more complex effect on confined concrete columns compared to unconfined concrete columns, because the confinements due to steel reinforcements and FRP jackets complicate the stress condition of the top/bottom regions of columns. Thus, the end friction should be taken into account when modeling FRP-confined concrete columns by numerical method.

Based on the experimental data presented in part I of these companion papers, a semi-empirical model is proposed for the axial stress-strain curves of aramid FRP-confined reinforced HSC columns with square cross-sections. In addition, a three-dimensional finite element model is developed by using the finite element software ANSYS. In the finite element model, a Drucker-Prager plasticity constitutive model and an elastic-plastic constitutive model are used for the confined concrete, and a linear elastic constitutive model is used for the FRP. A contact nonlinear is considered to simulate the end friction between the load platens of testing machine and the tested columns. Moreover, the influence of end friction is investigated with different parameters of height-width ratio of columns, amount of aramid FRP jackets, and amount of steel stirrups. In the part II of these companion paper, all the definitions and notations from the part I are retained.

2. Semi-empirical Model

2.1. Strain

For RC columns, the axial compressive strains of concrete core and the longitudinal steel reinforcements are both equal to the axial compressive strain of columns. Based on the experimental data (as shown in Table 3 in the part I of these companion papers), the relationship between the transitional compressive strain ratio ($\varepsilon_{t-p} / \varepsilon_{c0}$) and the confinement ratio (f_1 / f_{c0}) is computed by regression (a least-squares fit of data to a nonlinear line), as shown in Fig. 1(a). That is

$$\frac{\varepsilon_{t-p}}{\varepsilon_{c0}} = 1 + 6\left(\frac{f_1}{f_{c0}}\right)^2 \tag{1}$$

(a) Transitional compressive strain ratio   (b) Ultimate compressive strain ratio
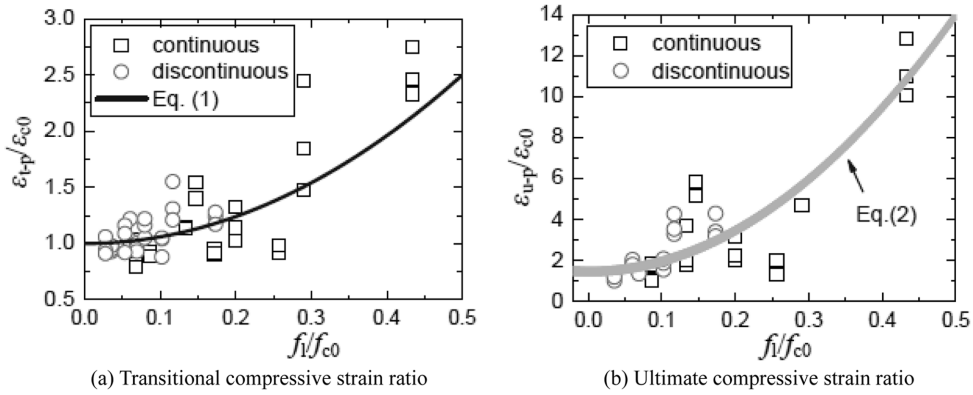
Fig. 1 Regression for transitional compressive strain ratio and ultimate compressive strain ratio
Note: "continuous" denotes the specimens confined with continuous AFRP wrapping, "discontinuous" denotes the specimens confined with discontinuous AFRP wrapping

The relationship between the ultimate compressive strain ratio ($\varepsilon_{u\text{-}p}$ / ε_{c0}) and the confinement ratio is also computed by regression, as shown in Fig. 1(b)

$$\frac{\varepsilon_{u-p}}{\varepsilon_{c0}} = \frac{\varepsilon_{u-p}^{c0}}{\varepsilon_{c0}} + 50\left(\frac{f_1}{f_{c0}}\right)^2 \tag{2}$$

It can be seen that there are good correlations between the experimental results and the proposed equations, with the regression coefficients (γ^2) in Eqs (1) and (2) equal to 0.73 and 0.81, respectively.

2.2. Strength

The transitional compressive strength of columns ($f_{t\text{-}p}$) can be obtained by superimposing a nominal transitional compressive strength of longitudinal steel reinforcements ($f_{t\text{-}p}^{sn}$) and a nominal transitional compressive strength of confined concrete core ($f_{t\text{-}p}^{cn}$); the ultimate compressive strength ($f_{u\text{-}p}$) can be also obtained by superimposing a nominal ultimate compressive strength of longitudinal steel reinforcements ($f_{u\text{-}p}^{sn}$) and a nominal ultimate compressive strength of confined concrete core ($f_{u\text{-}p}^{cn}$). That is

$$\begin{cases} f_{t\text{-}p} = f_{t\text{-}p}^{sn} + f_{t\text{-}p}^{cn} \\ f_{u\text{-}p} = f_{u\text{-}p}^{sn} + f_{u\text{-}p}^{cn} \end{cases} \tag{3}$$

As to RC columns, if the axial strain in the steel is less than the yield strain of steel, the stress in the steel is proportional to the strain; while if the strain is larger than the yield strain, the stress can be considered independent of strain and equal to the yield strength of steel (Spiegel and Limbrunner 1998). In this experiment, since the yield strain of longitudinal steel reinforcements is 1.3×10^{-3} and smaller than ε_{c0}, the longitudinal steel reinforcements have yielded when the axial stress-strain curve reaches its transitional point or ultimate point. Hence, the nominal transitional compressive strength and the nominal ultimate compressive strength of longitudinal steel reinforcements can be calculated by

$$f_{\text{t-p}}^{\text{sn}} = f_{\text{u-p}}^{\text{sn}} = f_{\text{yl}} \cdot \frac{A_{\text{sl}}}{A_{\text{cf}}} \qquad (4)$$

Shown in Fig. 2(a) is the relationship between the nominal transitional concrete strength ratio ($f_{\text{t-p}}^{\text{sn}}/f_{\text{c0}}$) and the confinement ratio, which exhibits monotone increase. Based on the experimental data, a regression formula is given as

$$\frac{f_{\text{t-p}}^{\text{cn}}}{f_{\text{c0}}} = \frac{f_{\text{t-p}} - f_{\text{t-p}}^{\text{sn}}}{f_{\text{c0}}} \cdot \frac{A_{\text{cf}}}{A_{\text{cf}} - A_{\text{sl}}} = 1 + 1.5\frac{f_{\text{l}}}{f_{\text{c0}}} \qquad (5)$$

Shown in Fig. 2(b) is the relationship between the nominal ultimate concrete strength ratio ($f_{\text{u-p}}^{\text{cn}}/f_{\text{c0}}$) and the confinement ratio, which also exhibits monotone increase. Based on the experimental data, a regression formula is given as

$$\frac{f_{\text{u-p}}^{\text{cn}}}{f_{\text{c0}}} = \frac{f_{\text{u-p}} - f_{\text{u-p}}^{\text{sn}}}{f_{\text{c0}}} \cdot \frac{A_{\text{cf}}}{A_{\text{cf}} - A_{\text{sl}}} = 0.7 + 3\frac{f_{\text{l}}}{f_{\text{c0}}} \qquad (6)$$

It can be observed that predictions from the proposed equations (Eqs. 5 and 6) agree well with the experimental results with the regression coefficients in Eqs (5) and (6) equal to 0.89 and 0.85, respectively.

2.3. Axial stress-strain curves

The cross sectional stress in FRP-confined reinforced HSC square column can be separated into two parts, one is the nominal compressive stress in the confined concrete core, and the other is the nominal compressive stress in the longitudinal steel reinforcements, as given by

$$\sigma = \sigma_{\text{cn}}\frac{A_{\text{cf}} - A_{\text{sl}}}{A_{\text{cf}}} + \sigma_{\text{sn}}\frac{A_{\text{sl}}}{A_{\text{cf}}} \qquad (7)$$

(a) Nominal transitional concrete strength ratio   (b) Nominal ultimate concrete strength ratio
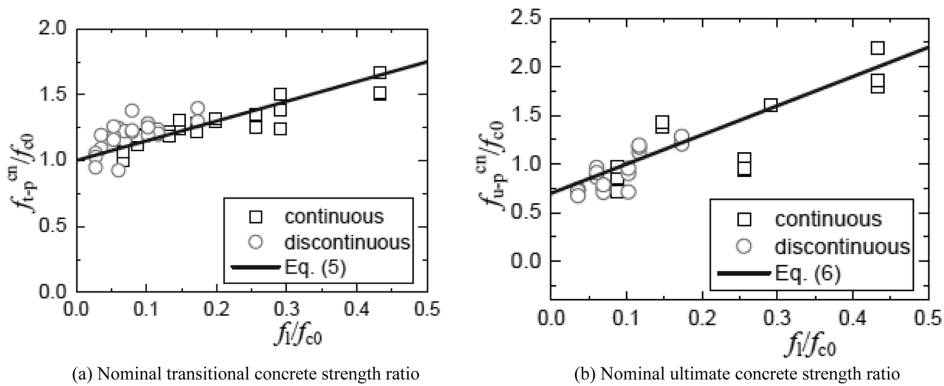
Fig. 2 Regression for nominal transitional concrete strength ratio and nominal ultimate concrete strength ratio Note: "continuous" denotes the specimens confined with continuous AFRP wrapping, "discontinuous" denotes the specimens confined with discontinuous AFRP wrapping

where σ_{cn} = nominal axial stress in the confined concrete core (MPa); σ_{sn} = nominal axial stress in the longitudinal steel reinforcements (MPa); The nominal axial strain of the columns (ε) is equal to that of the concrete core (ε_{cn}) and the longitudinal steel reinforcements (ε_{sn}).

To predict the stress-strain curves of confined concrete columns under concentric compressive loading, Richard and Abbott (1975) found, based on the experimental observations, that the axial stress-strain curves of confined concrete columns presented a shape of bilinear (i.e., a initial elastic states with higher modulus followed by a harden stages with lower modulus). A four-parameter formula was suggested, as follows

$$\sigma_{cn} = \frac{(E_1 - E_2)\varepsilon_{cn}}{\left[1 + \left(\dfrac{(E_1 - E_2)\varepsilon_{cn}}{f_0}\right)^n\right]^{1/n}} + E_2\varepsilon_{cn} \tag{8}$$

where E_1 = first slope of the curve (MPa); E_2 = second slope of the curve (MPa); n = curve-shaped parameter that mainly controls the curvature in transition zone; and f_0 = reference plastic stress at the intercept of the second curve with the axial stress (MPa), as shown in Fig. 3.

In order to make Richard and Abbott's formula adapted to reinforced HSC square columns confined by aramid FRP jackets, based on the experimental results and discussions presented above, the parameters of formula may be redefined as follows

$$E_1 = 3320\sqrt{f_{c0}} + 6900 \quad \text{[ACI-363 Committee (1984)]} \tag{9}$$

$$E_2 = \frac{f_{u\text{-}p}^{cn} - f_{t\text{-}p}^{cn}}{\varepsilon_{u\text{-}p}^{cn} - \varepsilon_{t\text{-}p}^{cn}} \tag{10}$$

$$f_0 = f_{u\text{-}p}^{cn} - E_2\varepsilon_{u\text{-}p}^{cn} \tag{11}$$

The compressive stress in the longitudinal steel reinforcements is given by

$$\sigma_{sn} = \begin{cases} E_{sl}\varepsilon_{sn} & (\sigma_{sn} < f_{yl}) \\ f_{sl} & (\sigma_{sn} \geq f_{yl}) \end{cases} \tag{12}$$
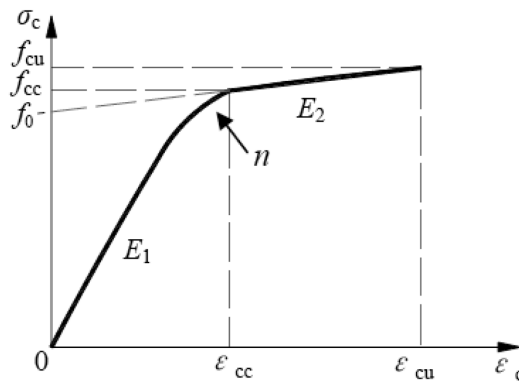

Fig. 3 Parameters of Richard and Abbott's formula

The complete axial stress-strain curves of reinforced HSC square columns confined by aramid FRP jackets can be obtained by substituting Eqs. (8) and (12) into Eq. (7). Shown in Fig. 4 are comparisons between the curves from the proposed model and the experiment. It can be observed that most of the predictions are in good correlation with the experimental data except for several groups (such as L-C-1 and M-C-3), a possible reason for which is the deviations in the regression analyses.
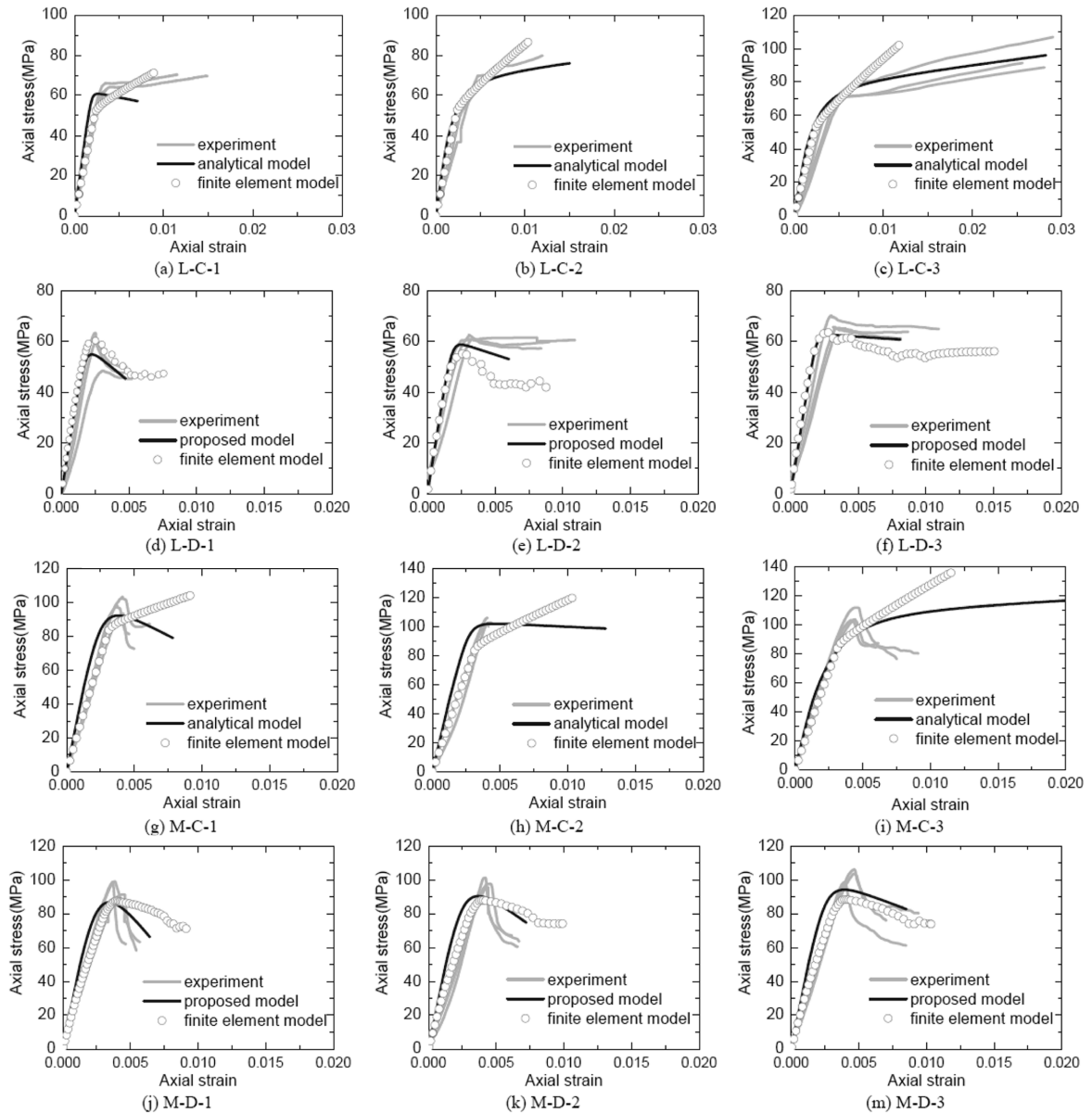

Fig. 4 Comparisons between predictions from semi-empirical model, finite element mode and experimental dada
Note: "experiment" denotes the experimental data; "proposed model" denotes predictions from the semi-empirical model; "finite element model" denotes predictions from the finite element model
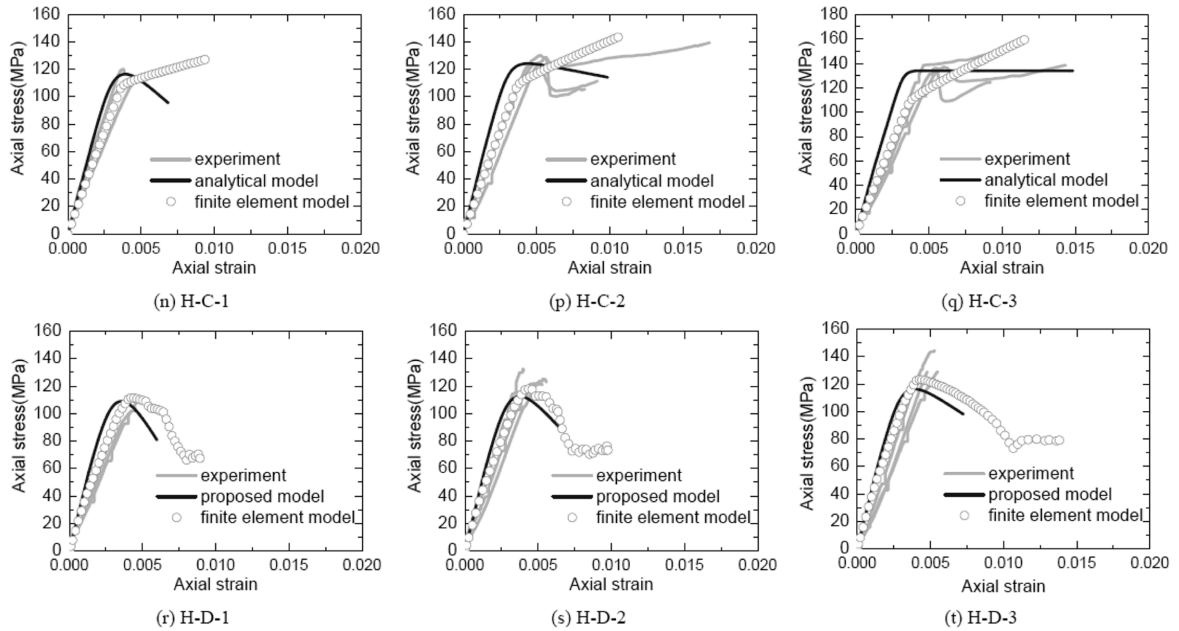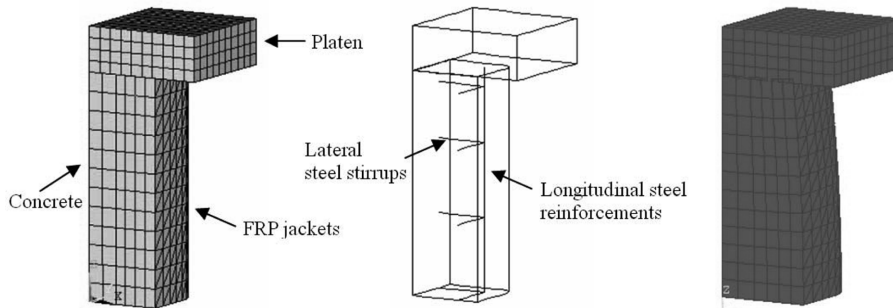
(n) H-C-1

(p) H-C-2

(q) H-C-3

(r) H-D-1

(s) H-D-2

(t) H-D-3

Fig. 4 Continued

Fig. 5 Discretization and deformation mesh of finite element model

3. Finite element model

3.1. Constitutive models of materials

3.1.1. Concrete

For the concrete core confined by internal steel stirrups and/or external aramid FRP jackets, its lateral dilation, which is activated by the compressive deformation in vertical (axial) direction, leads to passive lateral confining stress. Moreover, the internal steel stirrups provide constant confinement after they yield, while the external aramid FRP jackets provide increasing confinement until they break. Thus, the concrete core wrapped with aramid FRP sheets (called directly-confined concrete, as shown in Fig. 6 a) has sustained dilation until aramid FRP breaks and behaves similar to a plastic material; while the concrete core between adjacent aramid FRP sheets (called indirectly-confined concrete) behaves as an

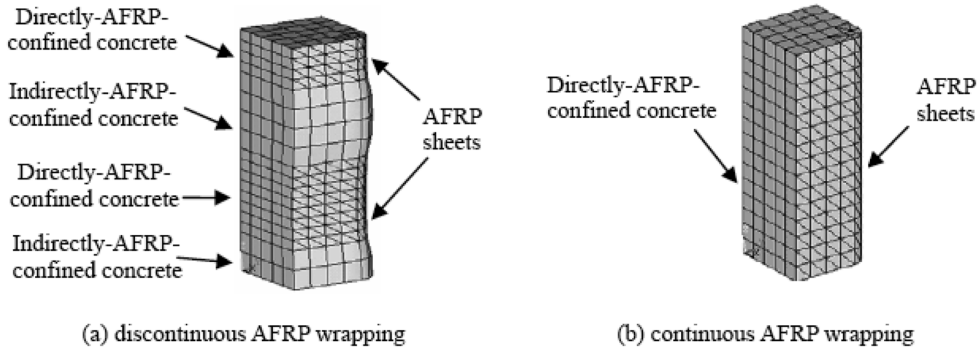(a) discontinuous AFRP wrapping   (b) continuous AFRP wrapping

Fig. 6 Deformed finite element mesh for HSC square columns confined with AFRP sheets

elastic-plastic material, since the confinement is distributed as arching along the vertical section of columns (Restrepo and De Vino 1995). Thus, a rational description for the dilation characteristics of confined concrete cores is important, and different concrete core need to be modeled by different constitutive material models.

In the finite element model developed herein, a Drucker-Prager plasticity constitutive model, which follows the classical theory of incremental plasticity, is selected to model the directly-confined concrete core. The cohesion and angle of internal friction for concrete can be related to concrete strength as (Mirmiran *et al.* 2000)

$$f_{c0} = \frac{2c \cos \phi}{1 - sin \phi} \tag{13}$$

$$k = \frac{1 + \sin \phi}{1 - \sin \phi} \tag{14}$$

where ϕ = angle of internal friction, which can be calculated from Eq. (13); c = cohesion, which can be gained as follows (Rochette and labossière 1996)

$$c = (f_{c0} - 5\sqrt{3})\frac{3 - \sin \phi}{6 \cos \phi} \tag{15}$$

k = confinement effectiveness factor and is given by

$$k = \frac{f_{cp} - f_{c0}}{f_1} \tag{16}$$

where f_{cp} = peak compressive strength of the confined concrete. Ansari and Li (1998) found the best fit value of k is 2.6. The initial Young's modulus of HSC is calculated from Eq. (9). The initial Poisson's ratio (v_c) is given by (Candappa *et al.* 2001)

$$v_c = 8 \times 10^{-6}(f_{c0})^2 + 0.0002f_{c0} + 0.138 \tag{17}$$

For the indirectly-confined concrete, an elastic-plastic constitutive model is used. This constitutive model can take both cracking and crushing failure modes into account, based on the Willam-Warnke failure surface (Willam and Warnke 1975). The uniaxial stress-strain relationship, used in the elastic-plastic constitutive model, is given by (Guo 1999)

$$\begin{cases} \dfrac{\sigma_c}{f_{c0}} = \alpha\dfrac{\varepsilon_c}{\varepsilon_{c0}} + (3 - 2\alpha)\left(\dfrac{\varepsilon_c}{\varepsilon_{c0}}\right)^2 + (\alpha - 2)\left(\dfrac{\varepsilon_c}{\varepsilon_{c0}}\right)^3 \ (\varepsilon_c \leq \varepsilon_{c0}) \\[4mm] \dfrac{\sigma_c}{f_{c0}} = \dfrac{\varepsilon_c}{\varepsilon_{c0}}\left[\beta\left(\dfrac{\varepsilon_c}{\varepsilon_{c0}} - 1\right)^2 + \dfrac{\varepsilon_c}{\varepsilon_{c0}}\right]^{-1} \qquad\quad (\varepsilon_c > \varepsilon_{c0}) \end{cases} \tag{18}$$

where the constant α and β are calculated by

$$\alpha = 2.77 - 0.029 f_{c0} \tag{19}$$

$$\beta = 7.26 f_{c0}^2 \times 10^{-4} \tag{20}$$

3.1.2. Steel and Aramid FRP materials

The longitudinal steel reinforcements and the lateral steel stirrups are assumed to be a perfect plasticity material, which means that the stress in the steel reinforcements continues to increase before they yield, and then keeps constant. The external aramid FRP is assumed to be a unidirectional linear elastic material, which means that the stress in the aramid FRP continues to increase until they rupture. In addition, as many researchers have pointed out, the maximum strain of FRP measured in FRP-confined concrete columns is lower than its ultimate rupture strain under pure tensile test (Xiao and Wu 1999, Lorenzis 2001). Thus, the maximum strain of aramid FRP jackets is assumed to be $0.65\varepsilon_f$, which is mainly caused by the stress concentration of FRP jackets when failing.

3.1.3. Platens of testing machine

The load platens of testing machine are assumed to be a rigid material. In the finite element developed in this paper, since no measurement was taken on the contact surface between the load platens and the tested specimens, the friction coefficient of contact surfaces is set as 0.47 (Baltay and Gjelsvik 1990).

3.2. Modeling

The finite element software ANSYS provides amount of elements for materials with different characters (ANSYS 2006). In the finite element model, the concrete core is modeled with SOLID65 element, which is a three-dimensional solid element with eight nodes, and capable of cracking in tension, crushing in compression, and accommodating plastic deformations. The lateral steel stirrups and the longitudinal steel reinforcements are modeled with LINK8 element, which is a three-dimensional spar element with two nodes at ends, and a uniaxial tension-compression element. The FRP jackets are modeled with SHELL41 element, which is a three-dimensional shell element with four (or three) nodes, and has membrane (in-plane) stiffness but no bending (out-of-plane) stiffness. The load platens of testing machine are model with SOLID185 element, which is a three-dimensional solid element with eight

nodes, and has mixed formulation capability for simulating deformations of nearly incompressible elastic-plastic materials or fully incompressible hyperelastic materials. In the finite element model, neither any slip between the concrete and the steel reinforcements, nor between the concrete and the aramid FRP jackets is considered. The principle direction of aramid FRP jackets is normal to the axial direction of columns, and the SHELL41 element is set as tension-only.

Meanwhile, a contact nonlinear is applied to model the end friction between the load platens of testing machine and the tested columns. In FEA, the "contact-target" pair concept has been widely used to simulate the contact between two bodies. It means that a surface of one body is taken as a contact surface, and a surface of other body is taken as a target surface (ANSYS 2006). For a rigid-flexible contact, the contact surface is associated with a deformable body, and the target surface must be subordinated to a rigid body. Therefore, in this study, the load platens of testing machine are treated as the rigid bodies, and their surfaces contacting the tested columns are modeled to the target surfaces by use of TARGE170 element; and the tested columns are treated as the flexible bodies and their surfaces contacting the load platens are modeled to the contact surfaces by use of CONTACT174 element.

The symmetries of geometry in the specimens and the load provide a permission that only a top quarter of the specimen needs to be considered in the finite element model (as shown in Fig. 5). Three symmetric planes are included as the boundary conditions. All nodes on each symmetric plane are fixed only in the direction normal to the plane. The axial load is treated as a displacement, which is applied to all nodes on the bottom surface of model.

3.3. Results

The three-dimensional nonlinear finite element model is run in ANSYS, and the end point of calculation is that the maximum strain in the aramid FRP jackets reaches $0.65\varepsilon_f$, as well as the steel stirrups yield. The axial stress-strain curves from the finite element model are shown in Fig. 4, which agree well with those from the experiment for most of specimens.

4. Influence of end friction

As to the influence of end friction, the value of friction coefficient is a key factor. Many researchers suggested their proper friction coefficient between steel plates and concrete specimens. Rabbat and Russell (1995) tested a friction coefficient between rolled steel plate and concrete with different normal compressive stress levels (between 0.14 and 0.69 MPa), and their experimental investigation showed that the average friction coefficient varied between 0.57 and 0.70. Baltay and Gjelsvik (1990) implemented experiment to determine a friction coefficient between steel and concrete with different normal compressive stress levels (between 0 and 468.52 MPa), and it was found that the average friction coefficient was 0.47. Malvar *et al*. (2004) considered the end friction by way of a restrained top or bottom surface of column, and their results showed that the end friction could increase the unconfined concrete compressive strength by up to 5.6%. Cairns *et al*. (2007) reported that a friction coefficient of steel/concrete interface was 0.55. Forquin *et al*. (2008) also gave a friction coefficient between steel and concrete equaled to between 0.0 and 0.1 when the concrete specimens were compressed at high rates of strain, mainly due to the fact that the interface was coated with Teflon.

In the following investigation, all the columns are reinforced HSC square columns confined with continuous aramid FRP wrapping. The compressive strength of columns is represented with a nominal

strength which is defined as P_{max} / A_{cf}, where P_{max} is the axial compressive load capacity of columns (kN). The compressive strain of columns is represented with a nominal ultimate strain which is defined as δ_{max} / h, where δ_{max} is the axial compressive deformation corresponding to P_{max} (mm), and h is the height of the columns (mm).

Shown in Fig. 7 is a typical distribution of end friction (that is the surface friction stress on concrete forced by the steel plate), on the top/bottom quarter surface of test specimen. It demonstrates that the end friction is more concentrated in the regions close to the corners of column.

Figs. 8~11 present the relationships between the friction coefficient (μ) and the nominal strength, between the friction coefficient and the nominal ultimate strain, on the condition of different factors: the height-width ratio of columns (h / d, where d is the width of the columns); the amount of aramid FRP jackets ($\rho_f = 4t_f d / A_{cf}$, where ρ_f is the reinforced ratio of aramid FRP jackets, and t_f is the thickness of aramid FRP jackets); the amount of steel stirrups [$\rho_{sh} = 4A_{sh}d / (A_{cf}S_h)$, where ρ_{sh} is the reinforced ratio of steel stirrups, A_{sh} is the cross-section area of the steel stirrups; and S_h is the center spacing of the steel stirrups]. In Figs. 8~11, ρ_{sl} is the ratio of the area of longitudinal steel reinforcements to the cross-section area of columns. In the following researches, except the aforementioned three factors (h / d, ρ_f and ρ_{sh}), the other parameters of columns were constant (that is, $d = 100$ mm, $R = d/10$, $f_{c0} = 80$ MPa, $f_f = 2060$ MPa, $E_f = 118 \times 10^3$ MPa, $f_{sh} = 265$ MPa, $E_{sh} = 2 \times 10^5$ MPa, $f_{sl} = 265$ MPa, $E_{sl} = 2 \times 10^5$ MPa, $\rho_{sl} = 0.0203$, respectively).

Fig. 8 presents the influences of end friction on the nominal strength and nominal ultimate strain, with
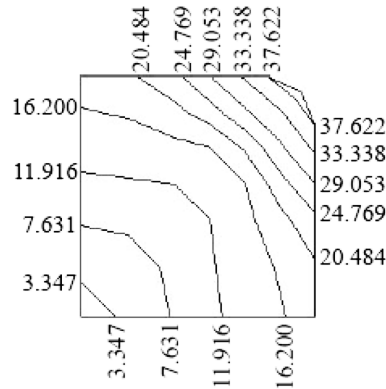

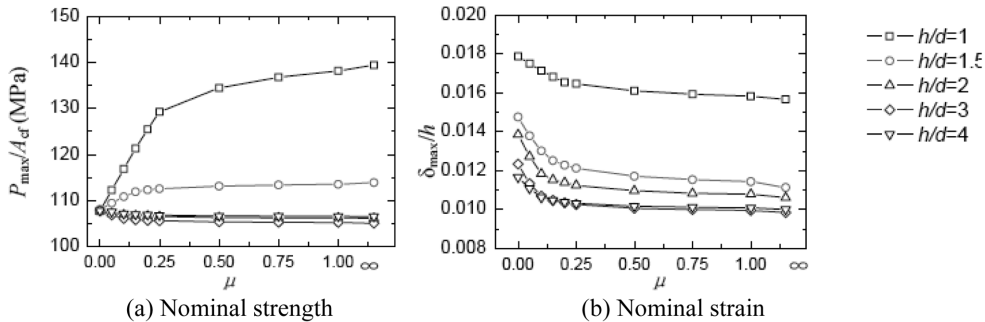Fig. 7 Typical distribution of the end friction (MPa)

(a) Nominal strength   (b) Nominal strain

Fig. 8 Effects of the end friction with different height-width ratio ($\rho_f = 0.0115$, $\rho_{sh} = 0.0101$)

the different height-width ratios (h / d) ranging from 1.0 to 4.0. It can be observed that the nominal strength notably increases with increasing the friction coefficient for $h / d = 1.0$ or 1.5, and the increments are 29.4% and 5.4% respectively, because a almost full-height additional lateral confining stress due to the end friction is brought on the columns. However, for $h / d = 2.0$, 3.0, and 4.0, the influence of end friction is unobvious and the nominal strength decreases slightly with increasing the friction coefficient, and the decrements are 1.4%, 2.5%, and 1.2% respectively, because the mid-height of columns is not subjected to the additional lateral confining stress. As far as the nominal ultimate strain, as shown in Fig. 8(b), it decreases with increasing the friction coefficient, and the decrements range between 12.4% and 24.5%. Meanwhile, the nominal ultimate strain almost keeps constant when $h / d \geq 3.0$. It means that a proper height-width ratio of aramid FRP-confined reinforced HSC square specimens is $h / d = 3.0$.

Figs. 9 and 10 present the influences of end friction with different amount of external aramid FRP jackets (ρ_f) ranging from 0.0115 (the thickness of aramid FRP jackets is 0.286 mm) to 0.0345 (the thickness of aramid FRPP jackets is 0.858 mm), or with different amount of internal steel stirrups (ρ_{sh}) ranging from 0.0101 (the diameter of steel stirrups is 4 mm) to 0.0912 (the diameter of steel stirrups is 12 mm) respectively. It is observed that the influences of end friction on the nominal strength are unobvious; the nominal strength decreases slightly with increasing the friction coefficient. The decrements of nominal strength range between 2.5% and 3.1% for different amount of external FRP jackets [as shown in Fig. 9(a)], and between 1.2% and 2.5% for different amount of internal steel stirrups [as shown in Fig. 10(a)]. However, the influences of end friction on the nominal ultimate strain are obvious; the nominal ultimate strain notably decreases with increasing the friction coefficient. The decrements of nominal ultimate strain range between 14.2% and 20.2% for different amount of external aramid FRP jackets [as shown in Fig. 9(b)], and between 13.2% and 20.2% for different amount of internal steel stirrups [as shown in Fig. 10(b)].

Fig. 11 presents the axial stress-strain curves of columns, with different friction coefficients. All the curves are bilinear and can be divided into two parts, that is, an elastic stage and a harden stage [as shown in Fig. 11(a)]. It also can be found that only the harden stages of curves are influenced by the friction coefficient [as shown in Fig. 11(b)], and the slope of harden stage increases as the friction coefficient increases.

In addition, Figs. 8~11 demonstrate that the nominal strength, the nominal ultimate strain, and the axial stress-strain curves are sensitive to the friction coefficient only when it ranges from 0.00 to 0.25. Therefore, for reinforced HSC square columns confined by aramid FRP jackets under concentric compressive loading, a proper friction coefficient of end friction is suggested to be a constant bigger than 0.25.
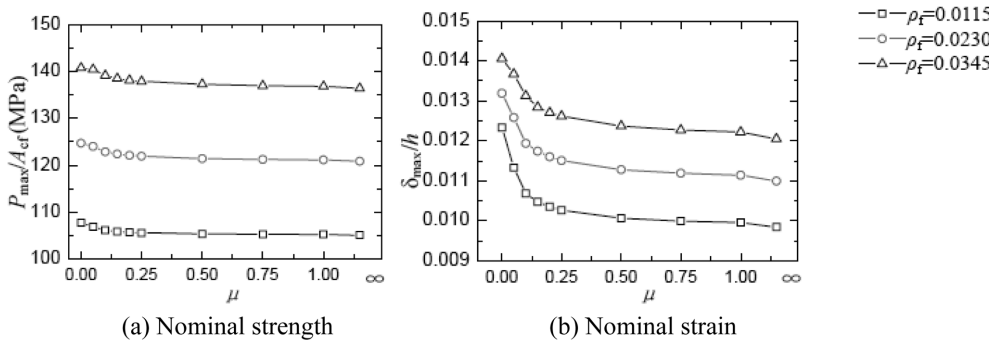

(a) Nominal strength   (b) Nominal strain

Fig. 9 Effects of the end friction with different amount of FRP ($h / d = 3$, $\rho_{sh} = 0.0101$)

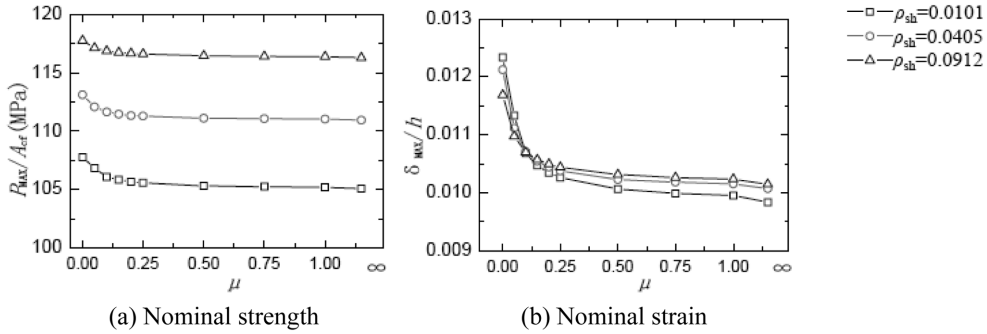(a) Nominal strength   (b) Nominal strain

Fig. 10. Effects of the end friction with different amount of steel stirrups ($h / d = 3$, $\rho_f = 0.0115$)

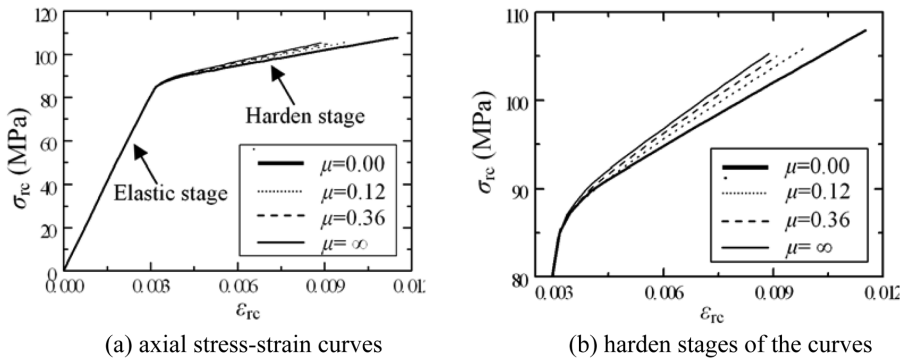(a) axial stress-strain curves   (b) harden stages of the curves

Fig. 11 Axial stress-strain curves with different friction coefficients ($h / d = 3$, $\rho_f = 0.0115$, $\rho_{sh} = 0.0101$)

5. Summaries and conclusions

1. The semi-empirical model, which is aimed to obtain the axial stress-strain curves, is adapted to the tested columns.

2. The three-dimensional nonlinear finite element model, which is developed to simulate the behaviors of the columns by using the finite element software ANSYS reproduces the experimental results.

3. The end friction is more concentrated in the regions close to the corners of columns.

4. The friction coefficient has notable influence on the nominal strength only when the height-width ratio of column is smaller than 3.0. The nominal ultimate strain decreases with increasing the friction coefficient, however it almost keeps constant when the height-width ratio is not smaller than 3.0. It means that a minimum height-width ratio of columns is 3.0.

5. With different amount of external aramid FRP jackets or internal steel stirrups, the influence of friction coefficient on the nominal strength is unobvious; on the other hand, the nominal ultimate strain notably decreases when the friction coefficient increases.

6. The axial stress-strain curves are only different in their harden stages with different friction coefficients. And the slope of harden stage increases as the friction coefficient increases.

7. The nominal strength, the nominal ultimate strain, and the axial stress-strain curves are sensitive to

the friction coefficient only when it ranges from 0.00 to 0.25. And a proper friction coefficient is suggested to be a constant bigger than 0.25.

7. Acknowledgment

Notation

The following symbols are used in this paper:

c	Cohesion for concrete material;
d	Width of the columns (mm);
A_{sl}	Cross-section area of longitudinal steel reinforcements (mm^2);
A_{cf}	Cross-section area of concrete confined by the AFRP jackets (mm^2);
f_0	Reference plastic stress at the intercept of the second stress-strain curve with the axial stress for concrete core (MPa);
f_{c0}	28-day average compressive strength of unconfined plain specimens (MPa);
f_{cp}	Peak compressive strength of the confined concrete (MPa);
$f_{t\text{-}p}$	Transitional strength for AFRP-confined reinforced HSC columns (MPa);
$f_{t\text{-}p}^{sn}$	Nominal transitional compressive strength of the longitudinal steel reinforcements (MPa);
$f_{t\text{-}p}^{cn}$	Nominal transitional compressive strength of the confined concrete core (MPa);
$f_{u\text{-}p}$	Ultimate strength for AFRP-confined reinforced HSC columns (MPa);
$f_{u\text{-}p}^{sn}$	Nominal ultimate compressive strength of the longitudinal steel reinforcements (MPa);
$f_{u\text{-}p}^{cn}$	Nominal ultimate compressive strength of the confined concrete core (MPa);
f_{yl}	Yield strength of longitudinal steel reinforcements (MPa);
f_l	Total equivalent confining stress (MPa);
E_1	First slope of stress-strain curve for confined concrete core (MPa);
E_2	Second slope of stress-strain curve for confined concrete core (MPa);
h	Height of the columns (mm);
n	Curve-shaped parameter that mainly controls the curvature in transition zone;
k	Confinement effectiveness factor;
P_{max}	Axial compressive load capacity of the columns (kN);
α	Concrete material constant;
β	Concrete material constant;
σ	Nominal axial stress (MPa);
σ_{cn}	Nominal axial stress in the confined concrete core (MPa);
σ_{sn}	Nominal axial stress in the longitudinal steel reinforcements (MPa);

ε — Nominal axial strain (m/m);

ε_{c0} — Compressive strain of unconfined plain specimens corresponding to f_{c0} (m/m);

ε_{cn} — Nominal axial strain of the concrete core (m/m);

ε_{sn} — Nominal axial strain of the longitudinal steel reinforcements (m/m);

ε_{f} — Ultimate strain of aramid FRP;

$\varepsilon_{t\text{-p}}$ — Transitional strain of AFRP-confined reinforced HSC columns (m/m);

$\varepsilon_{u\text{-p}}^{c0}$ — Ultimate strain of AFRP-confined reinforced HSC columns (m/m);

ρ_{f} — Ultimate strain of unconfined HSC columns (m/m);

ρ_{sh} — Reinforced ratio of aramid FRP jackets;

ρ_{sl} — Reinforced ratio of steel stirrups;

δ_{max} — Ratio of the area of longitudinal steel reinforcements to the cross-section area of the columns;

ϕ — Axial compressive deformation corresponding to P_{max}(mm);

ϕ — Angle of internal friction for concrete;

μ — Friction coefficient;

ν_{c} — Is the initial Poisson's ratio of concrete.

References

American Concrete Institute (ACI). (1984). "State of the art report of high-strength concrete." *ACI-363R-84*, ACI-363 Committee, Detroit.

Ansari, F., and Li, Q. (1998). "High-strength concrete subjected to triaxial compression." *ACI Mater. J.*, **95**(6), 747-755.

ANSYS Inc. Corporate. (2006). "The Ansys 10.0 user documents. http://www.ansys.com/services/ documentation/ index.htm.). (Nov. 2, 2007)

Baltay, P., and Gjelsvik, A. (1990). "Coefficient of friction for steel on concrete at high normal stress." *J. Mater. Civ. Eng.*, **2**(1), 46-49.

Braga, F., Gigliotti, R., and Laterza, M. (2006). "Analytical stress-strain relationship for concrete confined by steel stirrups and/or FRP jackets." *J. Struct. Eng.*, **132**(9), 1402-1416.

Campione, G. (2008). "Analytical model for high-strength concrete columns with square cross-section." *Struct. Eng. Mech.*, **28**(3): 295-316.

Candappa, D. C., Sanjayan, J. G.., and Setunge, S. (2001). "Complete triaxial stress-strain curves of high-strength concrete." *J. Mater. Civ. Eng.*, **13**(3), 209-215.

Cairns, J., Du, Y., and Law, D. (2007). "Influence of corrosion on the friction characteristics of the steel/concrete interface." *Constr. Build. Mater.*, **21**(1), 190-197.

Debaiky, A. S., Green, M. F., and Hope, B. B. (2007). "Modeling of corroded FRP-wrapped reinforcement concrete columns in axial compression." *J. Compos. Constr.*, **11**(6), 556-564.

Deniaud, C., and Neale, K. W. (2006). "An assessment of constitutive models for concrete columns confined with fibre composite sheets." *Compos. Struct.*, **73**(3), 318-330.

Eid, R., and Paultre, P. (2007). "Plasticity-based model for circular concrete columns confined with fiber-composite sheets." *Eng. Struct.*, **29**(12), 3301-3311.

Forquin, P., Gary, G., and Gatuingt, F. (2008). "A testing technique for concrete under confinement at high rates of strain." *Int. J. Impact Eng.*, **35**(6), 425-446.

Fujikake, K., Mindess, S., and Xu, H. (2004). "Analytical model for concrete confined with fiber reinforced polymer composite." *J. Compos. Constr.*, **8**(4), 341-351.

Grassl, P. (2004). "Modelling of dilation of concrete and its effect in triaxial compression." *Finite Ele. Ana.*

Design, **40**(9), 1021-1033.

Harajli, M. H. (2006). "Axial stress-strain relationship for FRP confined circular and rectangular concrete columns." *Cem. Concr. Compos.*, **28**(10), 938-948.

Karabinis, A. I., and Rousakis, T. C. (2002). "Concrete confined by FRP material: a plasticity approach." *Eng. Struct.*, **24**(7), 923-932.

Li, Y. F., Lin, C. T., and Sung, Y. Y. (2003). "A constitutive model for concrete confined with carbon fiber reinforced plastics." *Mech. Mater.*, **35**(3), 603-619.

Lin, H. J., and Liao, C. I. (2004). "Compressive strength of reinforced concrete column confined by composite material." *Compos. Struct.*, **65**(2), 239-250.

Lorenzis, L. D. (2001). "A comparative study of models on confinement of concrete cylinders with FRP composites." *Research Reference Prepared of Chalmers University Of Technology*, Goteborg, Sweden.

Maalej, M., Tanwongsval, S., and Paramasivam, P. (2003). "Modelling of rectangular RC columns strengthened with FRP." *Cem. Concr. Compos.*, **25**(2), 263-276.

Malvar, L. J., Morrill, K. B., and Crawford, J. E. (2004). "Numerical modeling of concrete confined by fiber-reinforced composites." *J. Compos. Constr.*, **8**(4), 315-322.

Mirmiran, A., Zagers, K., and Yuan, W. (2000). "Nonlinear finite element modeling of concrete confined by fiber composites." *Fininte Ele. Ana. Design*, **35**(1), 79-96.

Montoya, E., Vecchio, F. J., and Sheikh, S. A. (2004). "Numerical evaluation of the behaviour of steel- and FRP-confined concrete columns using compression field modelling." *Eng. Struct.*, **26**(11), 1535-1545.

Mosalam, K. M., Talaat, M., and Binici, B. (2007). "A computational model for reinforced concrete members confined with fiber reinforced polymer lamina: implementation and experimental validation." *Compos. Part B: Eng.*, **38**(5), 598-613.

Mukherjee, A., Boothby T. E., Bakis, C. E., Joshi, M. V. , and Maitra, S. R. (2004). "Mechanical behavior of fiber-reinforced polymer-wrapped concrete columns-complicating effects." *J. Compos. Constr.*, **8**(2), 97-103.

Parvin, A., and Jamwal, A. S. (2006). "Performance of externally of FRP reinforced columns for changes in angle and thickness of the wrap and concrete strength." *Compos. Struct.*, **73**(4), 451-437.

Parvin, A., and Wang, W. (2001). "Behavior of FRP jacketed concrete columns under eccentric loading." *J. Compos. Constr.*, **5**(3), 146-152.

Rabbat, B. G., and Russell, H. G. (1985). "Friction coefficients of steel on concrete or grout." *J. Struct. Eng.*, **111**(3), 505-515.

Restrepo, J. I., and De Vino, B. (1995). "Enhancement of the axial load carrying capacity of reinforced concrete columns by means of fiberglass-epoxy jackets." *Proc. of Advanced Composite Materials in Bridges and Structures II*, Montreal, 547-553.

Richard, F. E., and Abbott, B. J. (1975). "Versatile elastic-plastic stress-strain formula." *J. Eng.g Mech. Div.*, **101**(44), 511-515.

Rochette, P., Labossière, P. (1996). "A plasticity approach for concrete columns confined with composite materials." *Proc. of Advanced Composite Materials in Bridges and Structures*, CSCE, 359-366.

Rougier, V. C., and Luccioni, B. M. (2007). "Numerical assessment of FRP retrofitting systems for reinforced concrete elements." *Eng. Struct.*, **29**(8), 1664-1675.

Samaan, M., Mirmiran, A., and Shahawy, M. (1998). "Model of concrete confined by fiber composites." *J. Struct. Eng.*, **124**(9), 1025-1031.

Spiegel, L., and Limbrunner, G. F. (1998). *Reinforced concrete design*. Prentice Hall, USA.

Wang, Y. C., and Hsu, K.. (2008). "Design of FRP-wrapped reinforced concrete columns for enhancing axial load carrying capacity." *Compos. Struct.*, **82**(1), 132-139.

Wu, Han-liang, and Wang, Yuan-feng. (2010). "Experimental study on reinforce high-strength concrete short columns confined with AFRP sheets." *Steel Compos. Struct.*, **10**(6), 501-516.

Xiao, Y., and Wu, H. (2000). "Compressive behavior of concrete confined by carbon fiber composite jackets." *J. Mater. Civ. Eng.*, **12**(2), 139-146.

Youssef, M. N., Feng, M. Q., Mosallam, A. S. (2007). "Stress-strain model for concrete confined by FRP composites." *Compos. Part B: Eng.*, **38**(5), 614-628.

CC